Materials Research Express

INCLUSIVE PUBLISHING
TRUSTED SCIENCE

PAPER • OPEN ACCESS

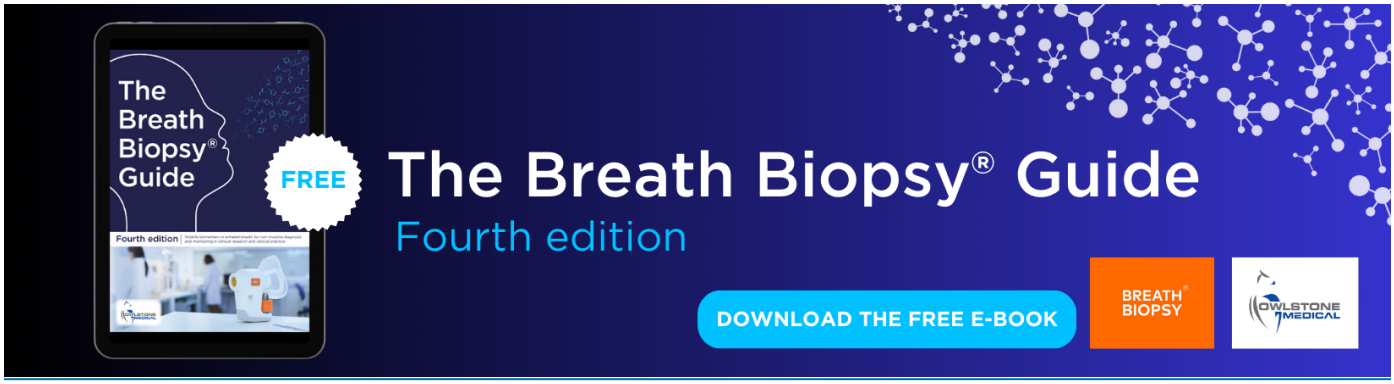
Experimental investigation of spin coating acceleration effect on the DSSC performance

To cite this article: Yusuf Yıldız *et al* 2024 *Mater. Res. Express* **11** 035502

View the article online for updates and enhancements.

You may also like

- Nanostructured perovskite oxides for dye-sensitized solar cells
Md Sariful Sheikh, Anurag Roy, Alo Dutta et al.
- Electrochemical Investigation of the Effect of Hydrogen Peroxide Concentration on Platinum-Particle-Assisted Etching of p-Type Silicon in a Hydrofluoric Acid Solution
Ayumu Matsumoto, Kyohei Furukawa, Shun Majima et al.
- One-step fabrication of effective mesoporous layer consisted of self-assembled MgO/TiO_2 core/shell nanoparticles for mesostructured perovskite solar cells
Lijia Che, Yanqun Guo, Chujian Liao et al.



This content was downloaded from IP address 95.183.211.218 on 14/04/2024 at 22:09

Materials Research Express

PAPER

Experimental investigation of spin coating acceleration effect on the DSSC performance

Yusuf Yıldız[1,2], Kemal Bilen[3] and Abdullah Atılgan[4]

[1] Department of Alternative Energy Sources Technology, GAMA Vocational School, Ankara University, Ankara, Turkey
[2] Graduate School of Natural and Applied Sciences, Faculty of Engineering and Natural Sciences, Ankara Yıldırım Beyazıt University, Ankara, Turkey
[3] Department of Mechanical Engineering, Faculty of Engineering and Natural Sciences, Ankara Yıldırım Beyazıt University, Ankara, Turkey
[4] Central Research Laboratory Application and Research Center, Ankara Yıldırım Beyazıt University, Ankara, Turkey

E-mail: ysfyildiz@ankara.edu.tr

Keywords: energy, solar energy, solar cell, spin coating, efficiency

OPEN ACCESS

RECEIVED
16 January 2024

REVISED
23 February 2024

ACCEPTED FOR PUBLICATION
6 March 2024

PUBLISHED
19 March 2024

Original content from this work may be used under the terms of the Creative Commons Attribution 4.0 licence.

Any further distribution of this work must maintain attribution to the author(s) and the title of the work, journal citation and DOI.

Abstract

The optimization of the TiO_2 mesoporous structure plays significant role in dye-sensitized solar cell (DSSC) to produce efficient devices. In this study, the TiO_2 mesoporous layer was coated by using a spin coating equipment with different spin accelerations. As a consequence of this investigation, the impacts of the spin coating acceleration on the optoelectronic and electrical performance characteristics of the DSSC were investigated. It has been shown that altering the spin coating acceleration has a direct impact on the mesoporous layer, which in turn influences the absorption ability of dye. The light absorbance of the sample A5 (coated at 2000 rpm s^{-1}) ascended drastically in accordance to other samples. Thanks to this augmentation in absorbance, the current density (J_{SC}) and power conversion efficiency (PCE) values also improved. According to electrochemical impedance spectroscopy analysis, it was attained that recombination resistance values increases with the rising spin coating acceleration rates after 500 rpm s^{-1} and reaches up to highest value at 2000 rpm s^{-1}. A relatively longer electron lifetime of 40.36 ms and recombination resistance of 12.22 Ω were obtained for the device coated at the rate of 2000 rpm s^{-1}. The device coated at a rate of 2000 rpm s^{-1} had a PCE (5.51%) that was superior than other devices because of its improved light collecting ability, quick electron transport, suppressed electron recombination, and having longer electron life time. As a starting point for future investigations and applications, results of present study provide an insight into the optimal spin coating parameters for DSSC applications.

1. Introduction

It is undeniable fact that the progression of humanity, science and technology are significantly reliant on energy. The development of clean renewable energy resources has been exhaustively studied as a means of reducing the rising energy needs and detrimental effects on the environment. Solar energy is foremost energy source among the numerous renewable energy sources due to its negligible environmental effect and widespread availability. The solar energy system utilizes sunlight to create power with no emissions that may hasten global warming.

Among the different solar energy studies, dye sensitized solar cells have been attracting rising interest last three decades thanks to their some of the benefits as affordable production techniques, good modification of device features, non-toxic material content, an environmentally friendly product structure, no harmful emissions, low cost processes etc [1–3]. DSSCs basically consist of four basic structures and studies are progressing on these structures in general. These structures are given as photoanode (PA) coated with a mesoporous TiO_2 nanoparticles, a molecular dye that absorbs the sunlight, electrolyte solution that creates a conducive atmosphere for the movement of electrons and a counter electrode (CE) which is platinum coated catalyst. Given that, a great deal of investigation has been done on each component/layer independently to

© 2024 The Author(s). Published by IOP Publishing Ltd

enhance the DSSCs' performance metrics [4]. The component of a DSSC that really determines how effectively light is harvested is called a dye sensitizer. So that, by choosing the dye in accordance to its light absorption ability in the visible region and compatible energy level with TiO_2, the performance of DSSC can be developed. Another important component of DSSC is electrolyte and it should have a high ion mobility to allow for quick charge transfer between the working and counter electrodes. In addition to dye and electrolyte, other important part of DSSC is the counter electrode. Its primary function is to draw electrons from an external circuit and catalyze redox reduction in the electrolyte. Therefore, catalytic activity of counter electrode should be high enough for a good device performance [5].

The photoanode (working electrode), another significant component of DSSC, serves two main purposes: it supports dye loading and facilitates the transfer of photo-excited charge carriers from the sensitized dye to the exterior circuit [6]. The photovoltaic performance of the DSSC is significantly influenced by the texture and composition of the semiconductor oxides that coated on photoanode. So that, significant research efforts have been made to examine the effects of photoanode modifications on DSSC performance. The modifications on photoanode can be separated into three distinct groups: doping with non-metallic anions and metallic cations, interfacial modification through the addition of blocking and scattering layers, and replacing the traditional mesoporous metal oxide films with one- or two-dimensional nanostructures [7, 8].

Apart from these studies on the photoanode, to optimize the photovoltaic performance of DSSCs, the experimental conditions can be altered without changing the main paste or fabrication ingredients. Su *et al* [9] studied on analysis and comparison of the impact of working temperature on the performance of the DSSC and hybrid device. They revealed that increasing temperatures causing low efficiencies a with decreasing open circuit voltage (V_{OC}). Atlı *et al* [10] fabricated the TiO_2 compact layer by changing the coating methods for developing the photoanode component of DSSCs. They used either soaking into a blue titania solution or by spin coating technique for covering the TiO_2 compact. Also, they studied on the effect of with/without a preheating treatment on the cell performance. Accordingly, utilizing a compact layer immersed in the solution and heated resulted in a significantly higher power conversion efficiency of 4.54%. Verjan *et al* [11] studied on the influence of temperature on particle size, porosity, and photovoltaic characteristics. According to photovoltaic results, the sample treated at 250 °C has better textural characteristics for the DSSC application. On the other hand, the highest power conversion efficiency of 6.43% attained at the sample treated at 150 °C. Jagtap *et al* [12] studied the impact of dye loading duration and binder content on a titania-based photoanode employed in a DSSC application. It has been observed that the cell performance noticeably changes when the TiO_2 photoanode is subjected to a long dye adsorption period. The result of the study demonstrates improved performance for 0.3 g of binder concentration and 90 min of dye loading time, with a maximum PCE of 5%. Rakhunde *et al* [13] investigated the influence of dye absorption duration of photoanode on the performance of ZnO basis DSSC. The ZnO seed layer was prepared using the doctor blade technique. DSSCs has been investigated at dye absorption times ranging from 60 to 240 min. The optimal dye absorption time for dye-sensitized ZnO photoanode has been determined to be 120 min. Chien *et al* [14] used the anthocyanin from red cabbage to create DSSC, and the best conditions for these device performance were investigated. The greatest power conversion efficiency (PCE) was attained with pH and anthocyanin extract concentrations of 8.0 and 3 mM, respectively, and with a 15-minute immersion period for producing sensitized TiO_2 film. Mehmood *et al* [15] added the graphene in the polyaniline matrix to produce a counter electrode. They varied the content of graphene from 6% to 15% for counter electrode fabrication. The total power conversion efficiency of the solar device made using 9% graphene composite counter electrode was found 7.45%. Gupta *et al* [16] used the Cu/S combination for co-doping the TiO_2 nanoparticles with constant ratio of 0.05% non-metal sulfur and various content from 0.1 to 0.5% of metal copper. After photovoltaic measurements, the device based on 0.05% sulfur and 0.3% copper co-doped TiO_2 displayed best PCE of 10.44% with remarkable augmented short circuit current density (J_{SC}) of 22.05 mA cm^{-2}. Najafabadi *et al* [17] studied on the fabrication of $BaSnO_3$ nanopowder by using co-precipitation method and applied this powders to substitute of photoanode material. They applied this powder with different values of calcination temperature and pH values to optimize the device performance. The best efficiency about 2.6% was perceived for the $BaSnO_3$ nanoparticles prepared within pH 12 and calcination temperature at 900 °C. Ningthoukhongjam *et al* [18] examined the effect of anatase/rutile (A/R) ratio of titanium photoanodes on the charge transport properties and power conversion efficiency. When compared to the other photoanodes, the DSSC with an A/R ratio of 1.44 found to be having greatest PCE. Khusaini *et al* [19] used the electrospinning machine for direct deposition of ZnO nanofibers on transparent conductive oxide (TCO) glass. They changed the stream velocity of electrospinning machine as 4, 6 and 8 μl min^{-1} to understand the its effects on ZnO nanofiber morphology. The results showed that the maximum efficiency that researchers reached on the stream velocity of 4 μl min^{-1} was 2.39%, 0.58 V open circuit voltage and 9.14 mA/cm^2 short circuit current density.

Generally, the researchers used the electrospinning or screen printing machine to coat the metal oxide paste. In this study, we used spin coating method to coat TiO_2 mesoporous layer as seen in figure 1. In contrast to prior

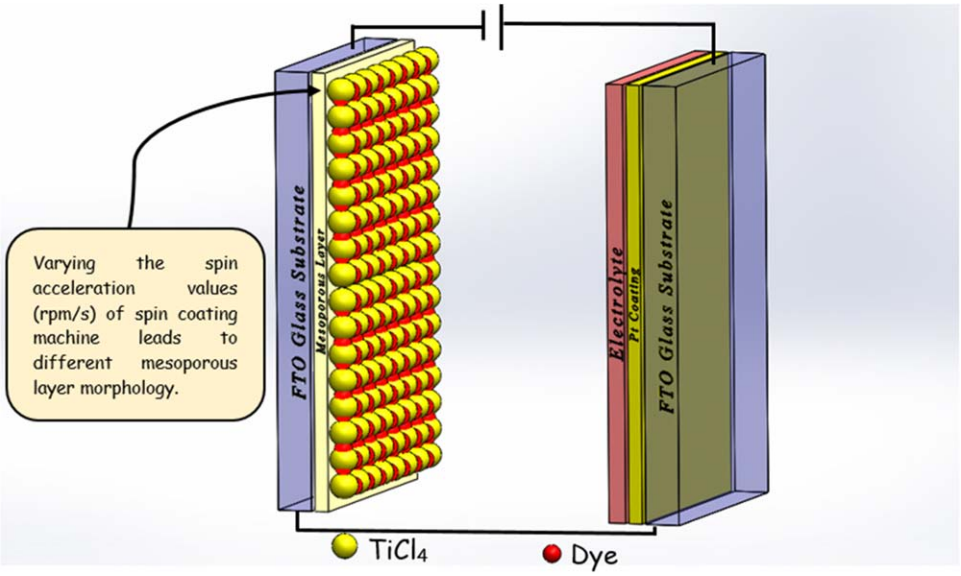


Figure 1. Three dimensional (3D) representation of designed solar cell device.

researches, we focused on the impact of spin coating acceleration on DSSC performance parameters. It is known that, spin coating acceleration affects the centrifugal force acting on the dropped paste solution. So, this force also impacts the homogeneous distribution of paste on TCO glass surface and determines the morphological features of mesoporous layer. To analyze the effect of spin coating acceleration values on the performance parameters of DSSC, we specified 5 different values ranging from 125 to 2000 rpm s^{-1}. The samples were entitled in accordance to acceleration rates as A1:125, A2:250, A3:500, A4:1000, A5:2000 rpm s^{-1}, A5 is the limit value which can safely be used in our machine. As a result of our study, we observed 10% of enhancement in PCE for the sample A5 compared to others. Based on our knowledge, this is the first study investigating the spin coating acceleration effect on the DSSC performance.

2. Experimental details

2.1. Producing of photoanode electrode

All chemical materials were used as received without any purification process. For coating process, fluorine doped tin oxide (FTO, Sigma Aldrich ~13 Ω sq^{-1}) substrates was selected as a transparent conductive oxide. These FTO substrates were firstly washed with dish soap to eliminate the adhering particles on the glass surface. After drying these glasses with an air pump, they depurated in ultrasonic bath by using ionized water, acetone (SigmaAldrich, 0.32201, 99.5%) and ethanol (Merck, 100 983, 99.9%). Afterwards, P25 nano-powders (Aeroxide TiO_2, Evonik), terpinol, and ethyl cellulose were used to synthesize a TiO_2 paste. In a nutshell, ethanol, P25 nano-powders, ethyl cellulose, and terpineol were mixed with specified ratios of (36:13.2:4:46. 8 wt%) to obtain a solution. A milky-like white slurry was produced by blending this mixture at 3500 rpm, 5 min in a mixer machine. To achieve a uniform surface, this solution was then spin coated onto FTO substrates during 30 s at 4000 rpm. While executing coating process, the acceleration values of machine was altered from 125 up to 2000 rpm s^{-1} as seen in figure 2. The samples were entitled in accordance to their spin coating accelerations as seen in table 1.

Following the coating the specimens, the porous TiO_2 morphology was formed by annealing the specimens for a half hour at 500 °C in order to remove the binding organic components adhering to surface of specimens. Following the application of this TiO_2 mesoporous layer, the samples were subjected to $TiCl_4$ post-treatment utilizing a straightforward bathing approach. For these post-treatments, $TiCl_4$ solution was diluted with deionized water to obtain an aqueous solution with a concentration of 100 mM. Using a magnet stirrer, solution was stirred for 30 min at room temperature to derive a homogeneous $TiCl_4$ solution. The photoanodes were subsequently exposed a chemical post-treatment by soaking in 100 mM solution at 70 °C for 30 min and then swashed with deionized water. Then, this $TiCl_4$ post-treated samples annealed at 450 °C for 30 min. By following the projected prescription, the essential photoanode, consisting of an FTO substrate, TiO_2 paste layer, and $TiCl_4$ post-treated layer was progressively achieved. Following sample coating procedures, photoanodes were

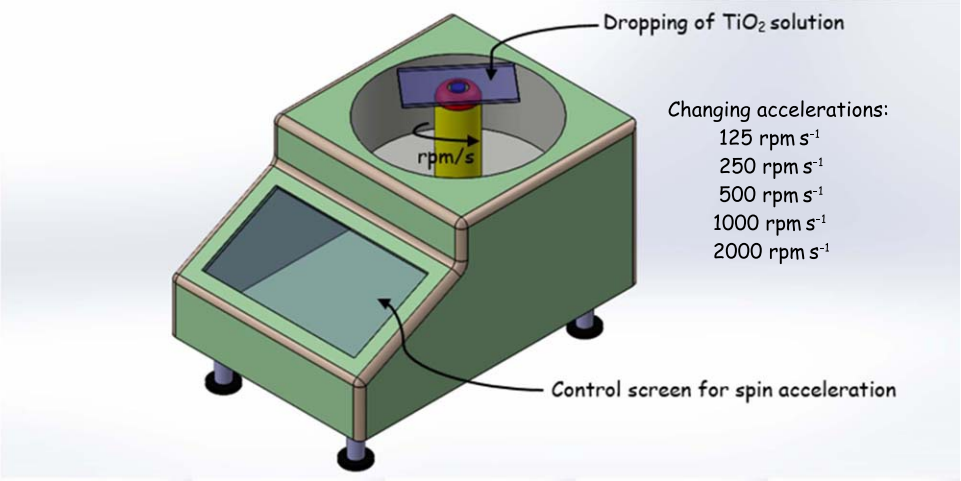


Figure 2. Demonstration of spin coating device and different acceleration values for TiO_2 coating.

Table 1. The changing parameters for coating of TiO_2 paste.

Samples	Spin acceleration (rpm s^{-1})	Acceleration time (s)	Coating speed (rpm)	Coating time (s)
A1	125	32	4000	30
A2	250	16	4000	30
A3	500	8	4000	30
A4	1000	4	4000	30
A5	2000	2	4000	30

immersed in a 0.3 mM N719 dye solution (dissolved in methanol) for 18 h and attained dye loaded samples as seen in figure 3.

2.2. Producing of counter electrode

FTO substrates were again used for counter electrode (photocathode) manufacturing process of solar cells. To fabricate the counter-electrodes, a Pt solution was prepared by dissolving 5 mM H_2PtCl_6 in isopropanol (IPA). This solution was then spin-coated onto bare FTO substrates at 2000 rpm, 2 s, 30 s. After that, they underwent a 30-minute annealing process at 400 °C.

2.3. Assemble of the devices

As mentioned above, after preparing the photoanode and counter electrode parts of solar cell, assembly of device was fulfilled to characterize the performance of devices. For short circuit current and voltage performance characterization of devices, a good photo catalytic electrolyte was used as electron source medium. The devices were filled with this electrolyte made of I_2 (0.05 M), LiI (0.1 M), 1-butyl-3-methylimidazolium iodide (BMII, 0.6 M), 4-tert-butylpyridine (TBP, 0.1 M), and acetonitrile. After filling the devices with the electrolyte, they were tightly assembled with the clamps and measurements were made to characterize the device performance parameters.

3. Characterizations

Schimadzu-UV 1700 was utilized to determine the photoanodes' optical properties. The I-V characteristics of assembled solar device, was analyzed by using a ABET (10500) Solar Simulator and Kiethley 2400 Sourcemeter. Electrochemical impedance spectroscopy (EIS) measurements carried out using a potentiostat (Gamry, interface 1000E), and the appropriate Gamry software was used to analyze the results. The thickness of TiO_2 layers and morphological characteristics of the samples have been investigated by employing a scanning electron microscopy (Hitachi SU5000 SEM). The illuminated active area was determined as 0.27 cm^2 with a mask under an incident solar power (AM 1.5, 100 mW cm^{-2}) generated by the solar simulator. The efficiency and power

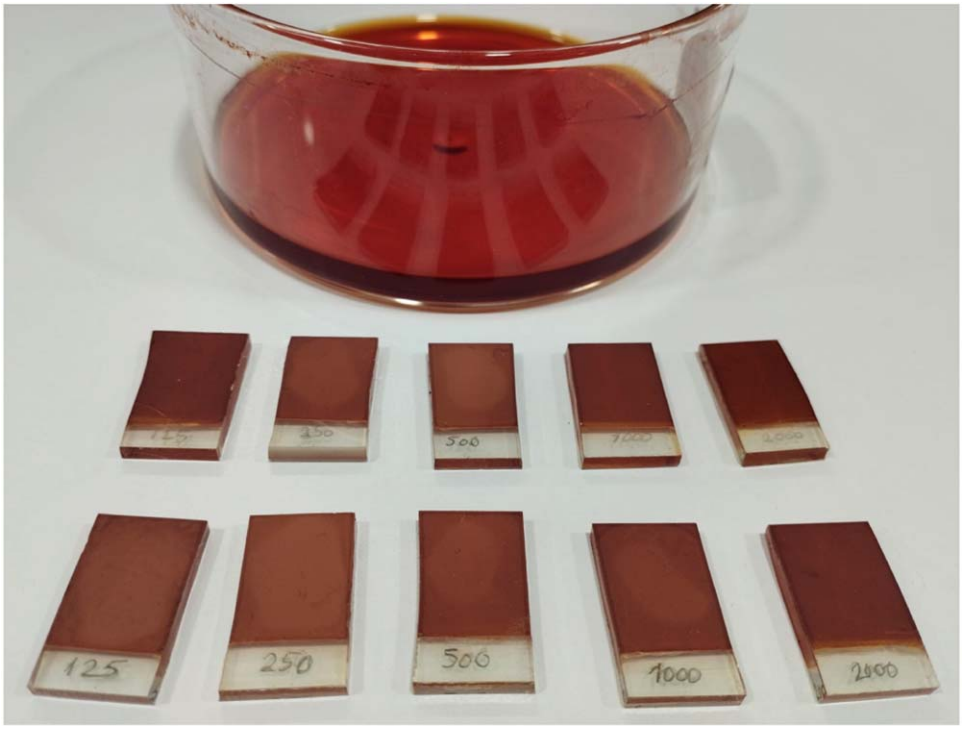


Figure 3. The photoanodes after 18 h dye loading procedure.

output of devices were measured under the standard conditions such as open air pressure, temperature of 24 °C, humidity of 43%.

4. Results and discussion

To investigate the thickness and morphology of the TiO_2 surfaces of samples prepared in different spin coating acceleration values, a Hitachi SU5000 type FE-SEM device employed. According to the cross-sectional images taken from FE-SEM, it was realized that the thickness of TiO_2 layers varied between 17.7 μm and 20.3 μm as seen in figure 4.

To exmaine the transparency of the samples transmittance measurements were executed after dye loading process. As expected, the transmittance values are inversely proportional to the absorbance values, and the results were found to be compatible with the trend of the absorbance values. While the sample A5 is showing a lowest transmittance, the sample A1 displays the maximum values of transmittance among the other samples as seen in figure 5.

To understand the dye absorption capabilities of the samples, the absorbance values of samples were measured in a UV–visible spectrophotometer (UV-1700 series from Shimadzu Corporation). To analyze the effect of dye on the optoelectronic properties of samples, two different measurements were made including before dye loading and after dye loading. Significant improvements in absorbance values of samples at a certain wavelength range, may be fulfilled by carefully altering the layer or coating conditions [20, 21].

As can be seen in figure 6, there is a remarkable increase in absorbance values after dye loading. When comparing the other samples that were fabricated at various accelerations, it should be noted that the sample A5, produced at 2000 rpm s^{-1}, had the maximum absorbance value after the dye loading process. The reason for having the highest absorption value for A5, may be attributed to obtaining the largest possible surface area thanks to the developing porous structure on TiO_2 layer as result of centrifugal force. It is known that if mesoporous TiO_2 nanoparticles have a larger interior surface area, the dye adsorption capacity enhances and promotes strong photocurrent production with excellent light absorption. Additionally, this mesoporous layer provides fast transmission of electrons at the device interface, which enhances the transmission of charge capabilities in a DSSC [22, 23].

To comprehend more detail, the delta absorbance ($\Delta A = A_{after\ dye} - A_{before\ dye}$) values were calculated for each sample and given in figure 7. To comment, it appears that the absorbance difference between samples increasing gradually from sample A1 to A5 and eventually this difference reaching the highest value for the sample A5. By increasing the acceleration values of spin coating device it was anticipated that TiO_2 porous

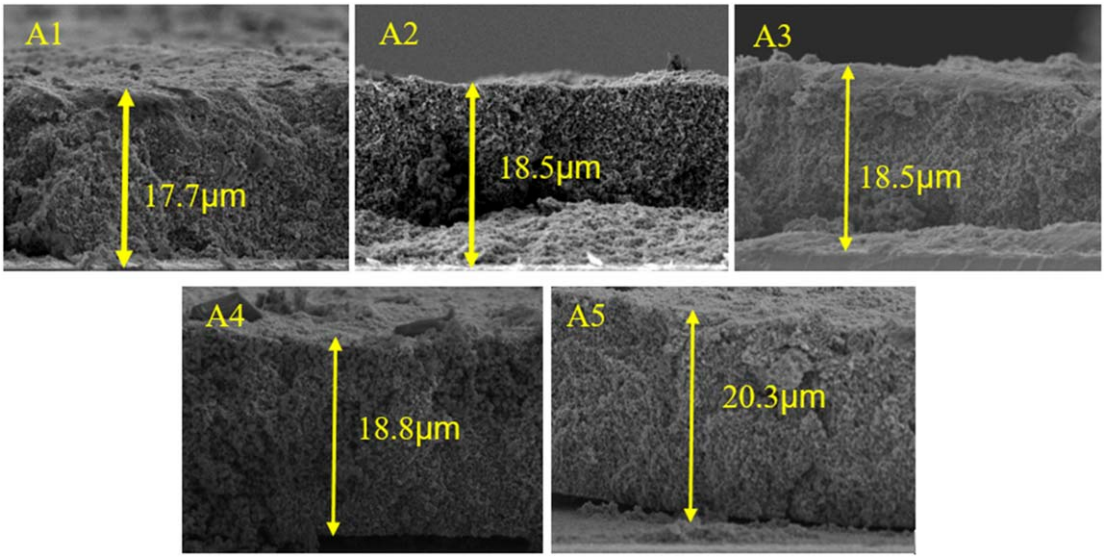


Figure 4. Cross-sectional FE-SEM images of TiO_2 samples prepared by spin coating at different spin accelerations.

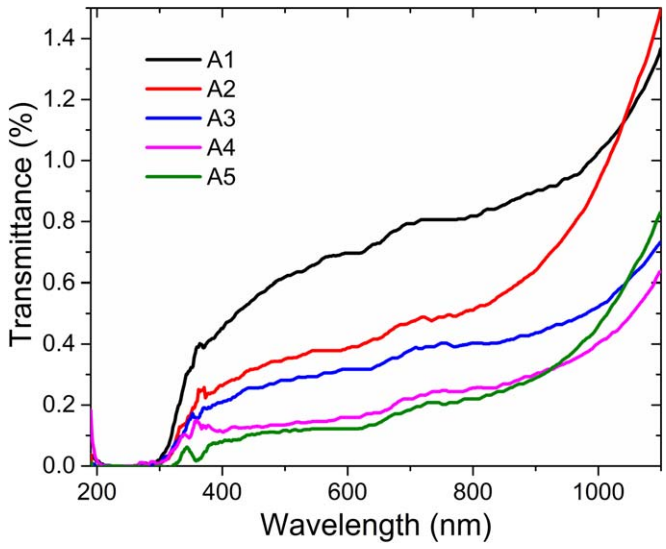


Figure 5. Transmittance spectra of the TiO_2 coated samples after dye loading.

structure developing and total surface area that the dye will adhere is increasing. This circumstance permits both significant dye-loading and improves charge collection efficiency by allowing more migrating carriers with enhanced light absorption/excitation [24].

To examine the optoelectronic parameters of samples the visible wavelength ranges of electromagnetic spectrum can be taken into consideration. The wavelength ranges at which photons coming from sun emit the highest energy is between 400 and 700 nm. In this wavelength range, the point where the highest irradiance value is reached is at 550 nm [25]. Therefore, the absorbance and transmittance values with respect changing spin acceleration values at 550 nm are given in figure 8. It can be clearly seen that absorbance values are increasing with rising acceleration values starting from 125 and increasing up to 2000 rpm s^{-1}. This increasing absorbance values are also indicator of the enhanced porous structure and increasing surface area of TiO_2 layer.

In addition to the optoelectronic parameters of a solar cell device, one of the other significant performance indicator of the matters that should be evaluated is interfacial charge transfer dynamics. To clarify the charge transfer dynamics of a solar cell device, it is important to perceive interfacial resistances from a Nyquist plot. In Nyquist plot, there is a vertically $Z''(\Omega)$ imaginary part shows the capacitive resistance values and a horizontally $Z(\Omega)$ real part of the graph shows the resistance in the circuit. These curves in the graph demonstrate the electrical losses in the solar cell layer structure, especially the horizontal part of this graph reflects the main idea

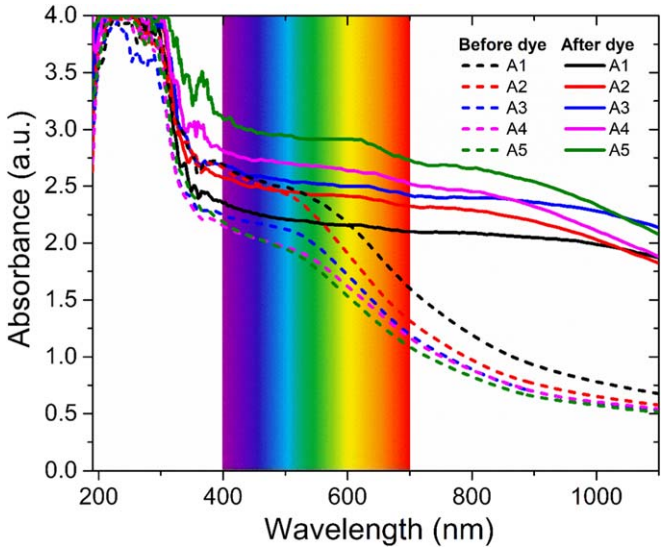


Figure 6. Absorbance spectra of the photoanodes before dye and after dye loading.

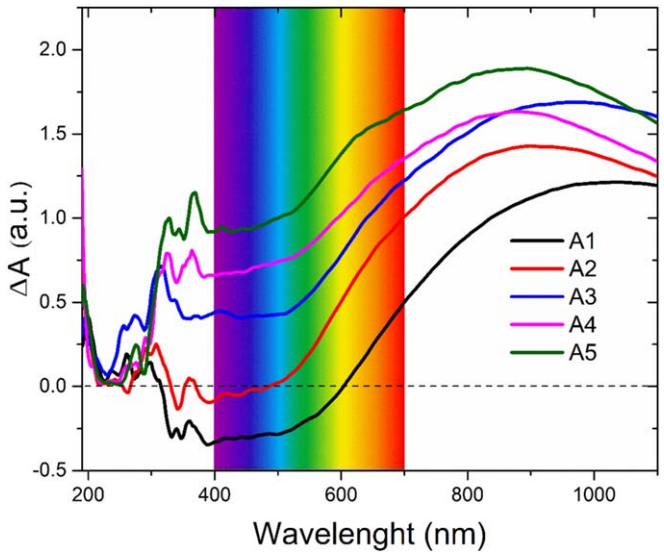


Figure 7. Delta absorbance spectra of the samples.

about the interfacial resistance values of devices. These interfacial resistance system is called as Nyquist equivalent circuit model and have been illustrated inset of figure 9. In a Nyquist plot, the great semicircle in lower frequency region is linked to the recombination resistance (R_r) at the TiO_2/dye/electrolyte contacts, whereas the minor semicircle in higher frequency region is in connection with the charge transfer resistance (R_C) at the Pt/electrolyte contact [1, 26, 27]. The source of series resistance (R_S) here is the FTO glass, which was chosen as substrate of the cells.

Accordingly, for a solar cell to perform well, the series and charge transfer resistance are expected to be low and the recombination resistance is expected to be high enough. Especially, to increase the number collecting electrons at the conduction band level of TiO_2/FTO and to prohibit the recombinations of electrons between layers of TiO_2/dye/electrolyte, recombination resistances should be greater.

As can be seen from the figure 9, the series resistance values of samples are almost the same as identical FTO glasses were used in all of the devices. First semi-circles indicate the charge transfer resistance (R_C), of which it can be also considered almost the same for all devices except little differences. These values cannot be easily distinguished from the graph but we can evaluate these parameters from table 2 with detail. On the other hand, recombination resistances (R_r) of samples can be clearly interpreted by looking into second semicircles given in

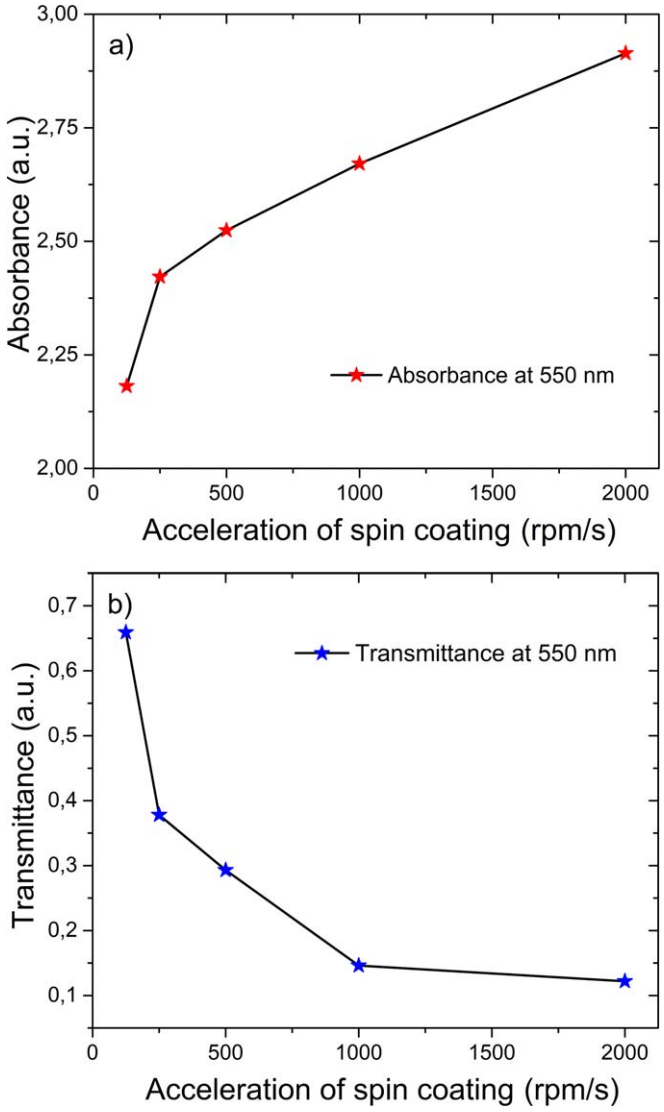


Figure 8. (a) Absorbance and (b) transmittance values of photoanodes at 550 nm wavelength.

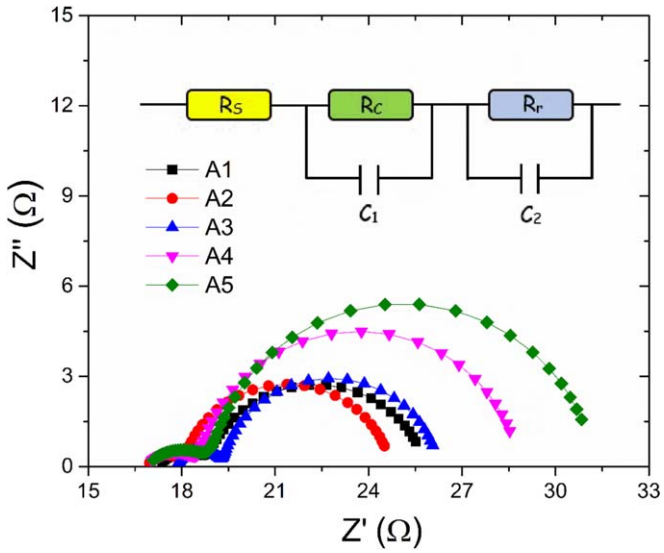


Figure 9. Nyquist plot of Electrochemical Impedance Spectroscopy (EIS) measurement and equivalent circuit model.

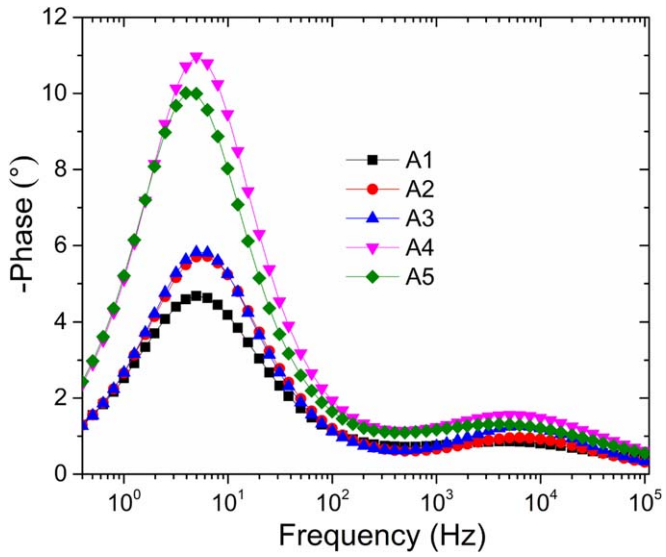


Figure 10. Bode plot of EIS measurement.

Table 2. Fitting results of EIS analysis for DSSCs.

Sample	R_s (Ω)	R_c (Ω)	R_r (Ω)	τ (ms)
A1	17.38	1.63	7.01	32.01
A2	16.97	1.16	6.67	25.04
A3	17.91	1.46	6.96	32.00
A4	17.05	1.68	10.25	32.05
A5	17.09	2.16	12.22	40.36

figure 9. The recombination resistance values augmented noticeably for sample A4 and A5, beyond the acceleration value of 500 rpm s^{-1} (sample A3).

To elucidate the effect of upgrading recombination resistance on solar cell device, electron life times attained from Bode graph was given detaily in table 2. Here, recombination resistance is accuried superior for the sample A5, indicating that the life time would be longer than the other samples. Considering the better absorbance value of sample A5, it seems to be compatible with the lifetimes and recombination resistance values here. Longer electron lifetime for the sample A5, supported with a low rate of charge recombinations by dint of rising recombination resistance. The provided parameters in table 2 correspond quite well with those that have been published in the literature [28, 29].

To calculate the lifetime values of electrons for each of sample, the Bode plot given in figure 10 was utilized. This figure displays the findings from Bode plot analyses of devices fabricated in five different spin coating acceleration values. Here, the characteristic frequency f_{max} (low-frequency peaks) is utilized to calculate the predicted lifetime of an electron (τ), which is oppositely correlated to f_{max}, in this Bode phase diagram. The electron lifetime is computed using the formula given below, where f_{max} is the greatest peak frequency at the counter electrode/electrolyte interface as illustrated in figure 10. The τ is defined by [30–32] as given in equation (1);

$$\tau = \frac{1}{2\pi f_{max}} \tag{1}$$

The electron lifetime of sample A5, which is 40.36 ms, is the greatest value among the other DSSCs, indicating that there is reduced recombination witn increasing recombination resistance of the device. Therefore, this rise in recombination resistance boosted the number of collected electrons in TiO_2 conduction band level and developed device performance.

To examine overall efficiency variation of a solar cell device, some of the main parameters as short circuit density (J_{SC}), open circuit voltage (V_{OC}), fill factor (FF) and power conversion efficiency (PCE, η) should be measured and analyzed. The J_{SC} value is the maximum current density that solar cells could generate and it is related to the amount of photons collected from light source. Also, V_{OC} is the highest voltage value a solar cell

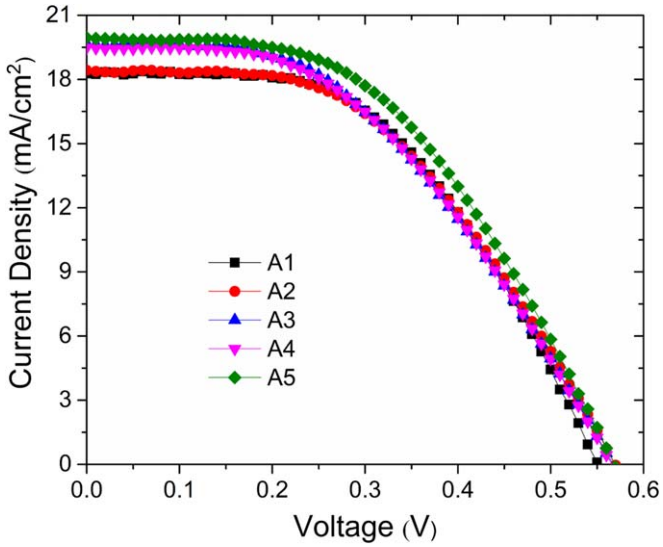


Figure 11. Current density versus voltage (J-V) graphs of the solar cell devices.

Table 3. Photovoltaic parameters of the DSSCs on different rpm values.

Sample	J_{SC} (mA cm^{-2})	V_{OC} (V)	FF (%)	η (%)
A1	18.28	0.550	0.50	5.03
A2	18.43	0.570	0.48	5.04
A3	19.69	0.568	0.45	5.03
A4	19.48	0.566	0.45	5.00
A5	19.96	0.569	0.48	5.51

can reach [33]. Nevertheless, the generated power of solar cell is zero at each of these working locations. The parameter that controls the maximum power output from a solar cell, along with V_{OC} and J_{SC}, is called the 'fill factor' or simply 'FF'. As shown in equation (2); the FF is defined as the ratio of the maximum power of solar cell to the product of V_{OC} and J_{SC}.

$$FF = \frac{P_{\max}}{J_{sc}\,V_{oc}} = \frac{J_{mpp}\,V_{mpp}}{J_{sc}\,V_{oc}} \tag{2}$$

Considering the graph, the FF represents the size of the greatest rectangle that would fit inside the J-V curve and serves as an indicator for the 'squareness' of a solar cell J-V graph.

The ratio of the maximal produced power (derived from equation (2)) to the incident power is used to compute the power conversion efficiency. A common method for determining the power conversion efficiency of solar cells is to use the irradiance value P_{in} of 1000 W/m^2 for the AM1.5 spectra, as shown in equation (3).

$$\eta = \frac{P_{\max}}{P_{in}} = \frac{J_{mpp}\,V_{mpp}}{P_{in}} = \frac{J_{sc}\,V_{oc}\,FF}{P_{in}} \tag{3}$$

As a consequence, the power conversion efficiency was obtained by gathering the measured data from the sourcemeter and using equations (2) and (3).

The current density versus voltage (J-V) graphs of the devices covering the different photoanodes of A1, A2, A3, A4 and A5 are shown in figure 11 and resulting photovoltaic characteristics are presented in table 3.

As seen in table 3, the device A5, with the pohotoanode that has been coated at 2000 rpm s^{-1}, has the greatest PCE of 5.51%, which is nearly 10% higher than the photoanodes coated at lower spin acceleration values.

The J_{SC} was improved with a rise from 18.28 mA cm^{-2} to 19.96 mA cm^{-2} when the spin coating acceleration values are raised as seen in figures 11 and 12(a). Three parameters should be considered by judging the magnitude of photocurrent density of the devices. These are light harvesting efficiency (LHE), electron injection efficiency (η_{INJ}) and charge collection efficiency (η_{COLL}). The LHE can be associated with dye loading capacity of the photoanodes. The η_{INJ} indicates how effectively the injection of the electrons from lowest unoccupied molecular orbital (LUMO) level of the dye to conduction band of TiO_2 occurs. To complete the circuit, finally,

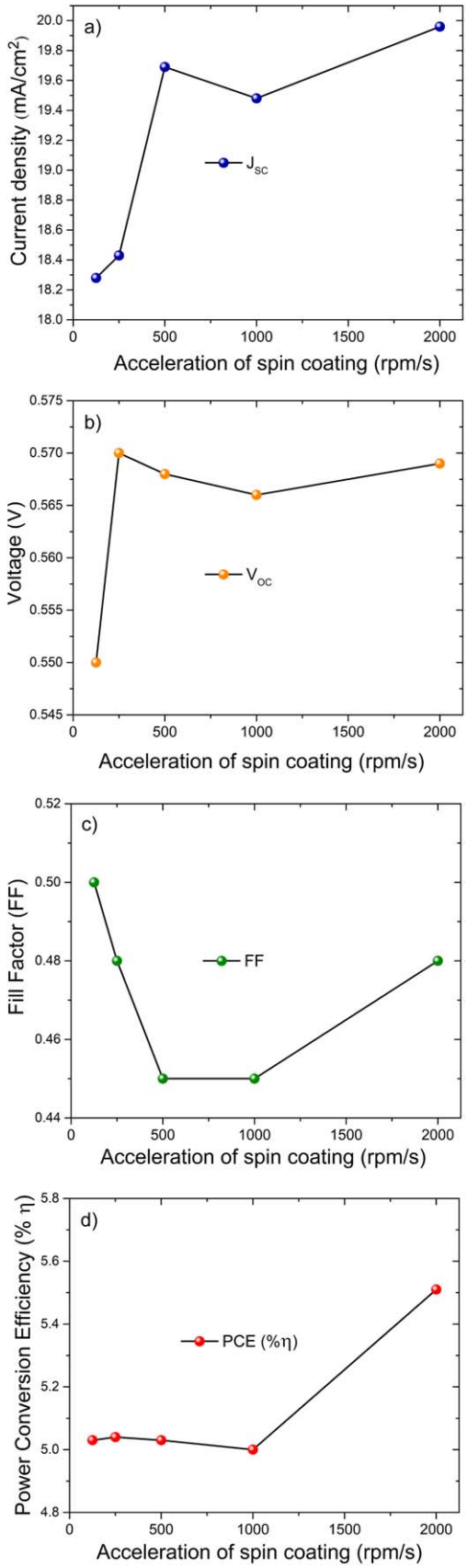


Figure 12. Demonstration of performance variations of devices with respect to spin acceleration. (a) *Jsc*, (b) *FF*, (c) *Voc*, (d) PCE versus acceleration of spin coating.

Table 4. Comparison of the performance results for DSSCs based on various deposition methods in the literature.

Deposition method	J_{SC} (mA/cm^2)	V_{OC} (V)	FF (%)	η (%)	References
Screen printing	3.16	0.624	0.72	1.43	[14]
Doctor blade	2.89	0.340	0.53	2.08	[13]
Doctor blade	11.77	0.673	0.50	3.94	[17]
Soaking technique	20.81	0.390	0.56	4.54	[10]
Doctor blade	6.20	0.66	—	5.37	[12]
Spin coating	19.96	0.569	0.48	5.51	This study
Hydrothermal treatment	18.59	0.729	0.47	6.43	[11]
Tape casting	15.60	0.788	0.62	7.63	[15]

the injected electrons must arrive at FTO, which is determined by η_{COLL}. In this study, since the morphology of the photoanodes is tailored by varying spin coating acceleration, one can expect that aforementioned three parameters can simultaneously play a role in determination of photocurrent density [34]. When looking at the voltage values, there is no significant change observed after 250 rpm s^{-1} as represented in figure 12(b). Another important parameter that determines the performance of solar cells is the fill factor (FF). This factor may differ according to the material properties known as shunt resistance or series resistance. In order to enhance the electron movement, it is expected that the shunt resistance should be high and the series resistance should be low in a material having quliafied crystal. In the study conducted here, it was seen that the fill factor was worse between 500 rpm s^{-1} and 1000 rpm s^{-1} values as illustred figure 12(c). So that, it seems more suitable to work with a spin coating device below 500 rpm s^{-1} or above 1000 rpm s^{-1} to get a better fill factor value by considering the other device performance parameters.

Finally, we need to evaluate the all these parameters by considering interconnections between them. Here, one metric might improve the device performance while the other deteriorates, hence it is more crucial to consider how these characteristics impact the overall device efficiency. When it was compared with the other devices, it turns out that the device A5 manufactured at 2000 rpm s^{-1} has a 10% higher efficiency than the others as demonstrated figure 12(d).

The DSSCs in this study were compared with previous reported DSSCs, whose structures contain spin coated TiO_2 mesoporous layer as shown in table 3. Based on the comparison in table 4, it can be inferred that our device exhibits better performance than many of other devices. Also, it can be deduced that the performance parameters of our device is compatible with those given in literature.

5. Conclusion

In this study, it was examined that the effect of spin coating acceleration on the TiO_2 mesoporous layer and device performance parameters. As a result, it was understood that the performance parameters of the solar cell was improved owing to the enhancement of the optoelectric and electrochemical properties of the TiO_2 coated photoanode. UV visible measurements show that the absorbance value of the sample A5 increased much more than the others when dye loaded. This remarkable increase in the absorbance value led to an increase in the J_{SC} value, which is one of the important performance parameters of the device, and ultimately an increase in efficiency. For the future studies, the used device in this study can be assembled with natural dyes which are alternative to N719 for non-toxic DSSC applications [35, 36]. In our future work, we aim to improve the performance of DSSCs, taking into account the experience and knowledge we have gained here. We predict that the results of this study will support and shed light on future studies using TiO_2 mesoporous layer for DSSCs.

Acknowledgments

This work is based on Yusuf YILDIZ's Ph.D thesis. The authors are thankful to stuff of Energy System Engineering Laboratory, for ensuring some facilities (UV-Vis spectrometer, I-V and EIS measurements) to perform a part of this investigation. This work is supported by the Ankara Yıldırım Beyazıt University BAP Coordination Unit, Turkey, under the project number 2372.

Data availability statement

All data that support the findings of this study are included within the article (and any supplementary files).

CRediT authorship contribution statement

Y. Yıldız: Sample preparation, Design of 3D shapes, Drawing of graphs, Writing original draft.
K. Bilen: Conceptualization, Methodology, Writing-review & editing, Supervision.
A. Atılgan: Experimental stage, Sample preparation, Measurements and characterizations.

Funding and/or conflicts of interests/competing interests

The authors declare that they have no known competing financial interests or personal relationships that could have appeared to influence the work reported in this paper. This work is supported by the Ankara Yıldırım Beyazıt University BAP Coordination Unit, Turkey, under the project number 2372. The authors express their gratitude to Ankara Yıldırım Beyazıt University BAP Coordination Unit for their support.

ORCID iDs

Yusuf Yıldız https://orcid.org/0000-0002-7635-0969
Kemal Bilen https://orcid.org/0000-0003-1775-7977
Abdullah Atılgan https://orcid.org/0000-0002-5624-3664

References

[1] Yildiz A, Chouki T, Atli A, Harb M, Verbruggen S W, Ninakanti R and Emin S 2021 Efficient iron phosphide catalyst as a counter electrode in dye-sensitized solar cells *ACS Appl. Energy Mater.* **4** 10618–26
[2] O'regan B and Grätzel M 1991 A low-cost, high-efficiency solar cell based on dye-sensitized colloidal TiO_2 films *Nature* **353** 737–40
[3] Akdogan N, Alp M, Atilgan A, Disli A, Erdogdu Y and Yildiz A 2023 An AZO dye with nitril anchoring to dye-sensitized solar cell performance: a theoretical and experimental investigation *Mater. Lett.* **351** 135075
[4] Atilgan A and Yildiz A 2022 Ni-doped TiO_2/TiO_2 homojunction photoanodes for efficient dye-sensitized solar cells *Int. J. Energy Res.* **46** 14558–69
[5] Sen A, Putra M H, Biswas A K, Behera A K and Groβ A 2023 Insight on the choice of sensitizers/dyes for dye sensitized solar cells: a review *Dyes Pigm.* **213** 111087
[6] Kumar S, Kumar S, Rai R N, Lee Y, Nguyen T H C, Kim S Y and Singh L 2023 Recent development in two-dimensional material-based advanced photoanodes for high-performance dye-sensitized solar cells *Sol. Energy* **249** 606–23
[7] Yeoh M E and Chan K Y 2017 Recent advances in photo-anode for dye-sensitized solar cells: a review *Int. J. Energy Res.* **41** 2446–67
[8] Sbeta M and Yildiz A 2019 Optical response enhancement of GZO/p-Si heterostructures via metal nanoparticles *Mater. Res. Express* **6** 085018
[9] Su S, Liu T, Wang Y, Chen X, Wang J and Chen J 2014 Performance optimization analyses and parametric design criteria of a dye-sensitized solar cell thermoelectric hybrid device *Appl. Energy* **120** 16–22
[10] Atli A, Sutcu I, Yildiz Z K and Yildiz A 2020 Optimizing deposition parameters of DSSCs composed of blue TiO_2 *IEEE J. Photovolt.* **11** 118–23
[11] González-Verjan V A, Trujillo-Navarrete B, Félix-Navarro R M, de León J D, Romo-Herrera J M, Calva-Yáñez J C and Reynoso-Soto E A 2020 Effect of TiO_2 particle and pore size on DSSC efficiency *Mater. Renew. Sustain. Energy* **9** 1–8
[12] Jagtap C V, Kadam V S, Mahadik M A, Jang J S and Pathan H M 2021 Effect of binder concentration and dye loading time on titania based photoanode in dye sensitized solar cell application *Engineered Science* **17** 133–41
[13] Rakhunde S S, Gadave K M, Shinde D R and Bhujbal P K 2020 Effect of dye absorption time on the performance of a novel 2-HNDBA sensitized ZnO photo anode based dye-sensitized solar cell *Engineered Science* **12** 117–24
[14] Chien C Y and Hsu B D 2013 Optimization of the dye-sensitized solar cell with anthocyanin as photosensitizer *Sol. Energy* **98** 203–11
[15] Mehmood U, Asghar H, Babar F and Younas M 2020 Effect of graphene contents in polyaniline/graphene composites counter electrode material on the photovoltaic performance of dye-sensitized solar cells (DSSCSs) *Sol. Energy* **196** 132–6
[16] Gupta A, Sahu K, Dhonde M and Murty V V S 2020 Novel synergistic combination of Cu/S co-doped TiO_2 nanoparticles incorporated as photoanode in dye sensitized solar cell *Sol. Energy* **203** 296–303
[17] Najafabadi H A, Fattahi A R, Asemi M and Ghanaatshoar M 2020 Performance enhancement of dye-sensitized solar cells by plasma treatment of $BaSnO_3$ photoanode. *J. Alloys Compd.* **818** 152856
[18] Ningthoukhongjam P, Bhagavathiachari M and Nair R G 2022 Effect of anatase-rutile phase ratio of titania photoanode on photoelectrochemical performance and photoconversion efficiency *Opt. Mater.* **127** 112269
[19] Khusaini M Z, Jati H N, Suyitno S, Hadi S and Arifin Z 2020 The influence of electrospinning flow rate parameter on ZnO nanofiber as photoanode of dye-sensitized solar cell In *AIP Conf. Proc.* **2217** 030096
[20] Atilgan A, Ozel K, Sbeta M and Yildiz A 2023 Engineering the visible light absorption of one-dimensional photonic crystals based on multilayers of Al-doped ZnO (AZO) thin films *Mater. Sci. Semicond. Process.* **166** 107747
[21] Yildiz Z K, Atilgan A, Atli A, Özel K, Altinkaya C and Yildiz A 2019 Enhancement of efficiency of natural and organic dye sensitized solar cells using thin film TiO_2 photoanodes fabricated by spin-coating. *J. Photochem. Photobiol.* A **368** 23–9
[22] Selvaraj P, Roy A, Ullah H, Sujatha Devi P, Tahir A A, Mallick T K and Sundaram S 2019 Soft-template synthesis of high surface area mesoporous titanium dioxide for dye-sensitized solar cells *Int. J. Energy Res.* **43** 523–34
[23] González-Verjan V A, Trujillo-Navarrete B, Félix-Navarro R M, León J D, Romo-Herrera J M, Calva-Yáñez J C, Hernández-Lizalde J M and Reynoso-Soto E A 2020 Effect of TiO_2 particle and pore size on DSSC efficiency *Mater. Renew. Sustain. Energy* **9** 1–8
[24] Atli A, Atilgan A and Yildiz A 2018 Multi-layered TiO_2 photoanodes from different precursors of nanocrystals for dye-sensitized solar cells *Sol. Energy* **173** 752–8

[25] Smets A, Jäger K, Isabella O, Van Swaaij R and Zeman M 2016 *Solar Energy: The Physics And Engineering Of Photovoltaic Conversion, Technologies And Systems* (Bloomsbury Publishing)
[26] Bilen K and Yildiz Y 2023 Synergistic effect of $Ga(NO_3)_3$ & $TiCl_4$ post-treatment on photovoltaic performance of dye-sensitized solar cells *Appl. Phys.* A **129** 310
[27] Atli A and Yildiz A 2022 Opaque Pt counter electrodes for dye-sensitized solar cells *Int. J. Energy Res.* **46** 6543–52
[28] Ilgün C, Sevim A M, Çakar S, Özacar M and Gül A 2021 Novel Co and Zn-Phthalocyanine dyes with octa-carboxylic acid substituents for DSSCs *Sol. Energy* **218** 169–79
[29] Lim S P, Pandikumar A, Lim H N, Ramaraj R and Huang N M 2015 Boosting photovoltaic performance of dye-sensitized solar cells using silver nanoparticle-decorated N, S-Co-doped-TiO_2 photoanode *Sci. Rep.* **5** 1–14
[30] Duan Y, Fu N, Liu Q, Fang Y, Zhou X, Zhang J and Lin Y 2012 Sn-doped TiO_2 photoanode for dye-sensitized solar cells *J. Phys. Chem.* **116** 8888–93
[31] Adriano S 2017 Electrochemical impedance spectroscopy: Fundamentals and application in dye-sensitized solar cells *Renew. Sustain. Energy Rev.* **79** 814–29
[32] Somdee A 2019 Improved photovoltaic efficiency of dye sensitized solar cells by decorating TiO_2 photoanode with barium titanate oxide *J. Alloys Compd.* **777** 1251–7
[33] Moghim M T, Jamehbozorgi S, Rezvani M and Ramezani M 2022 Computational investigation on the geometry and electronic structures and absorption spectra of metal-porphyrin-oligo-phenyleneethynylenes-[60] fullerene triads *Spectrochim. Acta* A **280** 121488
[34] Ghahramanpour M, Jamehbozorgi S and Rezvani M 2020 The effect of encapsulation of lithium atom on supramolecular triad complexes performance in solar cell by using theoretical approach *Adsorption* **26** 471–89
[35] Erdoğdu M, Atilgan A, Erdogdu Y and Yildiz A 2024 Natural dyes extracted from Ligustrum vulgare, Juniperus sabina, and Papaver rhoeas for novel DSSC applications *Mater. Lett.* **358** 135811
[36] Erdogdu M, Atilgan A, Erdogdu Y and Yildiz A 2024 Flavonoid from hedera helix fruits: a promising new natural sensitizer for DSSCs *J. Photochem. Photobiol.* A **448** 115288